JOURNAL OF APPLIED ELECTROCHEMISTRY 23 (1993) 257–264

Aluminium deposition and redissolution at TiB_2/C composite cathodes in cryolite based melts

S. C. RAJ*, M. SKYLLAS-KAZACOS

School of Chemical Engineering and Industrial Chemistry, University of New South Wales, P.O. Box 1, Kensington, NSW 2033, Australia

Received 23 March 1992; revised 26 August 1992

Electrochemical techniques of cyclic voltammetry and current reversal chronopotentiometry (CRC) with delay were used to evaluate the current efficiency of aluminium deposition together with its dissolution rates on TiB_2/C composite cathodes of $\leqslant 40$ wt % TiB_2 in NaF–AlF_3–Al_2O_3 molten baths. Experiments were conducted in both alumina-saturated and unsaturated melts. The working electrodes were titanium diboride-carbon composites and ATJ graphite. In general, the current efficiency for aluminium deposition was higher in unsaturated melts than in Al_2O_3-saturated melts. The rate of aluminium dissolution was found to be a diffusion-controlled process. The wettability of these composites by molten aluminium was found to be poor, this being attributed to the low surface TiB_2 content and the large graphite particles which prevent the formation of a thin continuous aluminium film on the surface of the cathodes.

Nomenclature

A	electrode area (cm^2)
b	slope of (τ_r/t_f) against t_d plots (s^{-1})
F	Faraday constant ($C\,mol^{-1}$)
$I\ (=I_f = I_r)$	applied current (A)
$I_d\ (=r_d AnF)$	dissolution current (A)
n	number of electrons
$Q_f = It_f$	cathodic charge (C)
$R\ (=\tau_r/t_f)$	limiting transition time ratio
r_d	dissolution rate for Al ($mol\,cm^{-2}\,s^{-1}$)
t_f	duration of deposition pulse (s)
τ_r	transition time corresponding to aluminium stripping (s)

1. Introduction

In the last forty years many organizations have patented processes pertaining to the development of cathodes that can be wetted by a thin film of molten aluminium [1–7]. The continued interest in inert cathodes has been sustained as a result of the recognition that inert, wettable cathodes could be utilized to reduce energy consumption in aluminium electrolysis [3]. The materials most commonly used are TiB_2/C-composites of various formulations [8].

As regards the wettability of the composite electrodes, laboratory-scale tests are needed to study the electrochemical behaviour of the composite materials. These tests are of fundamental importance in characterizing the extent of and the factors which affect the wettability of the electrodes and would provide insight into the behaviour of the electrodes in industrial applications. The purpose of this investigation is to study aluminium deposition and redissolution by electrochemical means at TiB_2/C-composite electrodes made up of 40% TiB_2, 12% large graphite particles and 48% carbon cement (COMP). Since carbonaceous materials also make up the electrodes, control experiments were also carried out with graphite electrodes. The investigations were carried out in both alumina-saturated and unsaturated cryolite-based melts, and the current efficiency for aluminium deposition was also determined.

2. Experimental details

The TiB_2/C composite materials used in this study were provided by Comalco Research Centre (Melbourne, Australia). In the composites, the TiB_2 powder was of the order of $\sim 40\,\mu m$ and the graphite filler particles were 0.5–2.5 mm. Graphite (ATJ grade, Carbon Brush Ltd., Sydney) was also used for comparison. For all the experiments in the alumina-saturated melt, the working electrodes (either COMP1, or ATJ Graphite) were encased in boron nitride (SBN Grade, ESK, Munich, West Germany) to define a specified circular area. The electrode was polished with SiC paper and 0.3 μm alumina, rinsed with acetone and subjected to ultrasonification. For all experiments in the unsaturated melts, the boron nitride sheath was eliminated and the electrode attached to a graphite connector to ensure that only the electrode material was in contact with the bath.

A tungsten wire electrode (1 mm diam. Alfa Products, Danvers, MA) was used as a quasi-reference electrode. The carbon crucible in which the electrolyte was contained served as the counter electrode.

* Present address: Environment Protection Authority New South Wales (EPA NSW), Locked Bag 1502, Bankstown, NSW 2200, Australia.

0021-891X

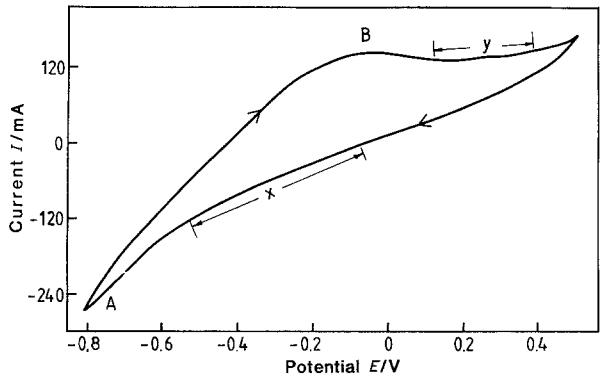

Fig. 1. Cyclic voltammogram, graphite electrode in Al_2O_3-saturated cryolite melt with 9.4 wt % Al_2O_3 and 5 wt % excess AlF_3, sweep rate = 100 mV s^{-1}, T_{im} = 11 h, A = 0.64 cm^2, melt temperature = 990° C.

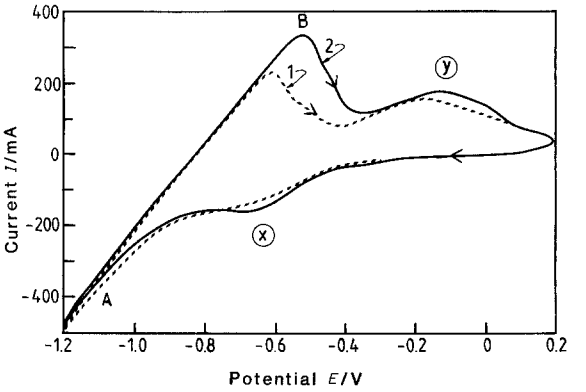

Fig. 2. Cyclic voltammogram, COMP electrode in Al_2O_3-saturated cryolite melt with 9.4 wt % Al_2O_3 and 5 wt % excess AlF_3, sweep rate = 100 mV s^{-1}, T_{im} = 75 min. Potential reversed at (1) −1.2 V, (2) −1.3 V. A = 0.64 cm^2, T = 990° C.

The other experimental details with respect to electrodes and electrochemical measurements are similar to those described elsewhere [3, 9].

Both alumina-saturated and unsaturated cryolite melts were used in this study. The melt compositions used were:

(A) 9.4 wt % Al_2O_3, 5 wt % xs-AlF_3, T = 990° C (Al_2O_3-saturated)

(B) 3.0 wt % Al_2O_3, 8% AlF_3, 5% CaF_2, T = 980° C (unsaturated)

According to the literature [10] the saturation concentration of melt A was about 10.7 wt % Al_2O_3 at 990° C. However, experimentally it was found that 9.4 wt % alumina was sufficient to achieve alumina-saturation at the cathode surface. Higher alumina contents resulted in solid cryolite formation at the surface of the working electrode.

3. Results and discussion

3.1. *Potential sweep experiments*

Figure 1 shows a typical cyclic voltammogram for the graphite electrode in an alumina-saturated melt after an immersion time (T_{im}) of 11 h. This voltammogram was obtained by starting the sweep from an open circuit voltage (o.c.v.) of −0.02 V in the cathodic direction at a sweep rate of 100 mV s^{-1}. The cathodic region, A, corresponds to aluminium deposition and anodic region B corresponds to reoxidation of the cathodically deposited aluminium. The increasing cathodic current in region X is attributed to sodium intercalation which precedes bulk deposition of aluminium at A [11]. Region Y represents de-intercalation of the sodium. The height of the aluminium stripping peak, (B), indicates poor wettability of the graphite substrate by liquid aluminium. The broadness of the stripping peak (B) indicates that aluminium is being stripped (and deposited) as a partially soluble product and/or as Na–Al alloy of varying activity [1]. However, the solubility of Na in Al is very low (0.13 wt %) and at the Al potential it is only about 150 p.p.m. [1, 2, 10]. Formation of aluminium carbide may also contribute to the broad nature of peak (B) because the reversible potential for aluminium carbide formation is 0.13 V positive to Al [1, 2, 10]. Simultaneous oxidation of aluminium carbide and aluminium could give a broad peak at B.

For the graphite electrode, cyclic voltammetric (CV) scans were done at intervals of 1–2 h over a total immersion time of 30 h. No oxidation peaks were observed up to a T_{im} of about 10 h indicating that aluminium deposition was not occurring for $T_{im} \leqslant$ 10 h. This phenomena was also noticed in a previous study [11] where it was shown that the graphite surface had to be saturated by sodium uptake before any aluminium deposition and subsequent reoxidation could be observed. This is consistent with observations made in industrial cells where there is preferential sodium penetration into the cathode lining in a new cell [1].

Figure 2 shows CVs for experiments with the COMP electrode in the alumina-saturated melt; aluminium deposition occurs in region A and reoxidation in region B. The stripping peak is broad for the same reasons as those outlined for the graphite electrode. In other similar experiments with the COMP electrode, peak B did not appear at all although the electrolysis time was extended up to 20 h. This inconsistency in electrochemical behaviour of the composite electrode is partly attributed to the heterogeneous nature of its substrate. Pure TiB_2 is readily wetted by liquid aluminium in cryolite-alumina melts [3, 7] whereas carbon-based materials are generally nonwettable [1, 2]. Since the COMP electrode consists of both wettable and nonwettable components, the overall wettability depends on the amount of TiB_2 particles in direct contact with the molten cryolite-alumina bath. It is also believed [12] that a carbon film exists on the surface of the electrode after it is polished. This originates from the pyrolysis of the phenolic resin binder during high temperature treatment of the composite. It is likely that this film also contributes towards hindering the wettability because in some experiments wettability increased with immersion time (i.e. with the number of cycles) and this could be related to the dissolution of the carbon film from the surface of the TiB_2 particle, by Al_4C_3 formation.

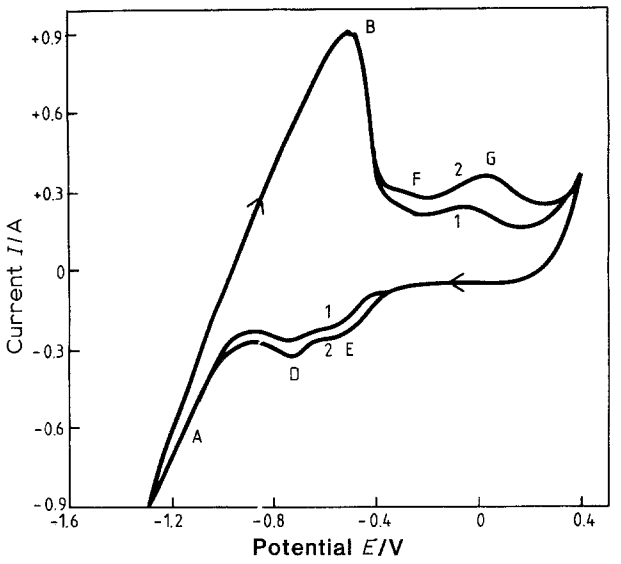

Fig. 3. Cyclic voltammogram for the COMP electrode in unsaturated cryolite melt with 3 wt % Al_2O_3, 8 wt % AlF_3, 5 wt % CaF_2, sweep rate = 200 mV s^{-1}, T_{im} = 0–15 min. (1) First cycle, (2) steady-state conditions. A = 0.64 cm^2, T = 980° C.

For all experiments in the alumina-saturated melt, the COMP electrode tended to be nonwettable initially. However, wettability increased with electrolysis time (T_{im}) in some experiments, whereas in others the electrode remained nonwettable throughout the electrolysis. However, once wettability was achieved in an experiment, then the electrode remained wettable throughout electrolysis and generally its wettability increased with immersion time. Overall, it was noticed that wettability was only achieved in about 20% of the experiments conducted in the alumina-saturated melts. In this study the distinction between the electrodes being wettable or nonwettable is based on whether peak B appeared or not.

Figures 3 and 4 show cyclic voltammograms for the COMP electrode in the unsaturated melt. It is evident that the behaviour of the electrode has changed significantly from that in the alumina-saturated melt. In Fig. 3, aluminium deposition occurs at A and reoxidation at B. The significance of the other peaks will be discussed later, but it is evident that aluminium deposition and reoxidation is occurring much more readily in the unsaturated melt as compared to the Al_2O_3-saturated melt. There are two possible reasons for this. It is now well established that there is a shift in the cryolite ratio at the electrode surface during electrolysis. It has also been observed [13] that in an alumina saturated melt the kinetics of alumina dissolution are slow enough for some particulate alumina to accumulate within the diffusion layer and interfere with the diffusion processes. It is also suspected that other particulates, such as cryolite precipitated from the electrolyte, also inhibit mass transport within the diffusion layer in the same manner as alumina. This accumulation of particulates close to the electrode surface inhibits the inward diffusion of the aluminium producing ions, AlF_6^{3-} and AlF_4^- and hence the current efficiency for aluminium production is expected to be lower in an Al_2O_3-saturated melt.

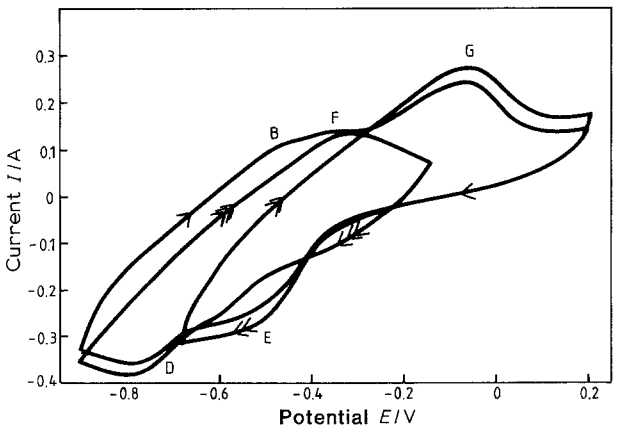

Fig. 4. Cyclic voltammogram for the COMP electrode in unsaturated cryolite melt with 3 wt % Al_2O_3, 8 wt % AlF_3, 5 wt % CaF_2, sweep rate = 200 mV s^{-1}, A = 0.64 cm^2, T = 980° C.

It is also known that B_2O_3 is used as a protective blanket to prevent possible oxidation of TiB_2 during curing [14]. If the oxidation of TiB_2 were to occur then it would occur via Equations 1 and 2 [15–19]:

$$TiB_2(s) + \tfrac{5}{2}O_2(g) = TiO_2(s) + B_2O_3(l) \quad (1)$$

$$B_2O_3(l) = B_2O_3(g) \quad (2)$$

Of the two oxidation products obtained via Reaction 1 it is known that B_2O_3 is not wetted by liquid aluminium [12] whereas TiO_2 has been found to be surface active and improves the wetting of carbon by liquid aluminium in a cryolite bath [15]. However, the non-wettability of B_2O_3 is not expected to be a problem in industrial cells as B_2O_3 has unlimited solubility in unsaturated melts and is not a detrimental impurity up to a concentration of 0.02 wt % [15]. However, B_2O_3 would not be able to dissolve rapidly in a saturated melt, and hence the electrodes would be expected to have poor wettability. This also explains why aluminium reoxidation peaks were not observed up to a certain T_{im} in the Al_2O_3-saturated melt in some experiments and why no peaks were observed in others. It is proposed that the slow dissolution of B_2O_3 prevented any wetting until a certain amount had dissolved at a certain T_{im}. As the B_2O_3 is gradually removed by dissolution, the concentration of TiB_2 at the composite surface increases. After a certain time, no more B_2O_3 would dissolve into the bath and the cyclic voltammogram exhibits steady-state behaviour. Generally, the dissolution of B_2O_3 in cryolite may take place according to one or both of Equations 3 and 4 [15]:

$$2Na_3AlF_6 + B_2O_3 = 2BF_3 + 6NaF + Al_2O_3$$

$$\Delta G^\circ_{1330\,K} = +129\ kJ\ mol^{-1} \quad (3)$$

$$Na_3AlF_6 + \tfrac{2}{3}B_2O_3 = \tfrac{4}{3}BF_3 + 2NaF + NaAlO_2$$

$$\Delta G^\circ_{1330\,K} = +295\ kJ\ mol^{-1} \quad (4)$$

The calculated value of Gibbs energy, ΔG° at 1330 K for Reactions 3 and 4 confirm that B_2O_3 does not dissolve readily into the cryolite melt. Further, since Al_2O_3 is formed by Reaction 3 the solubility of

B_2O_3 is expected to decrease with increasing content of Al_2O_3 dissolved in the cryolite melt. This also explains why the dissolution rate of B_2O_3 is very slow in an alumina-saturated melt.

Referring to Figs 3 and 4 again, two smaller cathodic peaks, D and E, are seen positive of the major deposition process and the corresponding anodic peaks are seen at F and G, respectively.

These peaks were first observed when the melts were changed from alumina-saturated to unsaturated (with respect to alumina) and were also observed in an earlier study at pure TiB_2 electrodes [17]. Detailed studies with the COMP electrode has confirmed that the cathodic prewaves D and E are observed even during the first potential sweep which is started from the o.c.v. in the cathodic direction (curve 1, Fig. 3). Further, the height of both the prewaves increases for subsequent sweeps after the electrode has been scanned to anodic region F and G, and then stabilises (curve 2, Fig. 3). From the above it can be concluded that the prewaves are associated with the reduction of products formed during the preparation and polishing of the electrodes, and further that more of these products are formed when the electrode has been scanned to anodic potential regions, for example region F and G in Fig. 3. Detailed studies with pure TiB_2 electrodes have shown [17] that the prewaves D and E represent the reduction of Ti^{4+} and B^{3+}, respectively. It is likely that oxidation of surface TiB_2 particles occurred via Equation 1 during machining of the TiB_2/C tiles to make small electrodes. The heat generated by friction might be enough to facilitate the oxidation. It is also likely that both TiO_2 and B_2O_3 were present in the matrix of the electrodes as impurities. Oxidation of TiB_2 in the composite could also occur by the CO_2 gas generated at the anode and is probably enhanced in anodic region F and G in Fig. 3 via Equation 5:

$$TiB_2(s) + \tfrac{5}{2}CO_2(g) = TiO_2(s) + B_2O_3(l) + \tfrac{5}{2}C(s) \quad (5)$$

This may explain why the height of the prewaves D and E increased after the electrode had been scanned to region F and G in Fig. 3. This also has very important implications for the aluminium industry. It has been envisaged that reducing the anode–cathode distance in the industrial cell may result in some oxidation of the TiB_2 in the composite material by the anodically generated CO_2 when the composite is used as a cathode in industrial cells. It is suspected that this may have deleterious effect on the wetting of the cathode by liquid aluminium. However, the present study with the COMP electrode has shown that a continuous potential sweep to positive potentials does not affect the subsequent aluminium deposition process in the unsaturated melt. Any oxidation of TiB_2 by the anode gas, thus seems to be a reversible process in the unsaturated melt. Since TiO_2 is a surface active oxide [15], its formation via Equation 1 may counter some of the adverse effects of B_2O_3 and carbon formation via the same reaction.

The magnitude of the peak current for both the cathodic waves D and E was found to be proportional to the square root of scan rate, $v^{1/2}$. This indicates that both the reactions represented by the two prewaves are solution reactions [20] and involve a diffusion process. A typical I_{pc} against $v^{1/2}$ curve for prewave D for the COMP electrode is shown in Fig. 5.

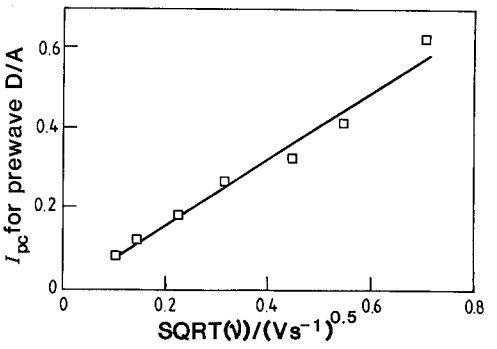

Fig. 5. Variation of I_{pc} for prewave D with square root of scan rate for the COMP electrode in unsaturated cryolite melt with 3 wt % Al_2O_3, 8 wt % AlF_3, and 5 wt % CaF_2 at 980° C. (□) Experimental; (——) regressed.

A further insight into the origin of prewaves D and E is obtained by comparing Figs 1 and 2. It is evident that under the same experimental conditions, prewaves D and E do not appear if a composite electrode is replaced by one made of graphite. This shows that the origin of D and E is intrinsically related to the TiB_2 component of the composite electrodes.

3.2. *Current reversal chronopotentiometry with delay*

Current reversal chronopotentiometry (CRC) with delay enables the rate of aluminium dissolution at open circuit potentials to be obtained more accurately than CRC [9] by introducing a delay time, t_d, at zero current between the cathodic and anodic current pulses. A series of current reversal chronopotentiograms with varying t_d is shown in Fig. 6 for the COMP electrode in an Al_2O_3-saturated melt. For each forward electrolysis pulse (t_f) there exists a reverse transition (τ_r) at zero volts and this corresponds to aluminium reoxidation. Similar trends were also observed for the graphite electrodes. Figures 7 and 8 show the relationship between (τ_r/t_f) and t_d for the COMP electrode in

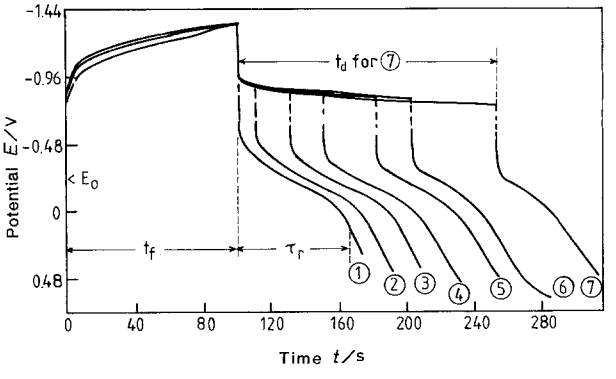

Fig. 6. CRC with delay, COMP electrode in alumina-saturated cryolite melt with 9.4 wt % Al_2O_3 and 5 wt % excess AlF_3, I = 0.7 A, A = 0.64 cm^2, T = 990° C. Delay, t_d: (1) 0, (2) 10, (3) 30, (4) 50, (5) 80, (6) 100, and (7) 150 s.

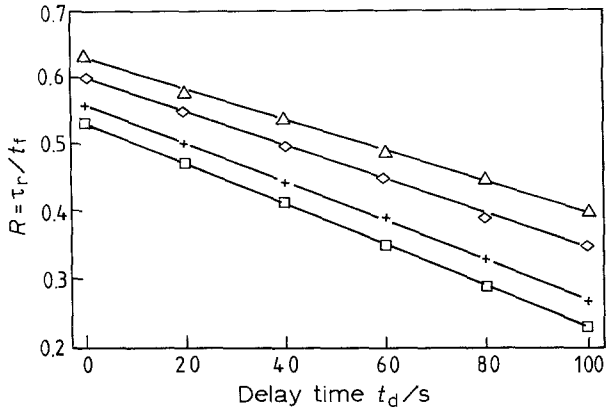

Fig. 7. Plots of (τ_r/t_f) against t_d for the COMP electrode in alumina-saturated cryolite melt with 9.4 wt % Al_2O_3 and 5 wt % excess AlF_3 at 990° C. $A = 0.64\,cm^2$. Current, I: (□) 0.3, (+) 0.5, (◇) 0.7, and (△) 1.0 A.

the Al_2O_3-saturated and unsaturated melts, respectively. In each case (τ_r/t_f) decreases linearly with delay time.

The rate of aluminium dissolution, r_d, can be determined from the slope of the (τ_r/t_f) against t_d plots [9, 11]:

$$r_d = b(Q_f/AnF)\,\text{mol cm}^{-2}\,\text{s}^{-1} \quad (6)$$

The dissolution rates for both electrodes in Al_2O_3-saturated and unsaturated melts are shown in Tables 1 and 2, respectively.

During aluminium deposition, the cryolite ratio at the electrode surface is changing and is greater than that in the bulk of the electrolyte [21]. Increasing the current density results in rapid build up of Na^+ at the cathode surface (i.e. the cryolite ratio at the cathode builds-up faster), and this results in an increase in dissolution rates [22, 23]. It can be seen that dissolution rates increase with applied current for CRC with delay experiments. This can be explained by examining the dissolution reaction:

$$Al(l) + 3Na^+ = 3Na(soln) + Al^{3+} \quad (7)$$

Equation 7 represents the predominant dissolution mechanism in basic melts (CR > 3). As the forward current applied is increased, the equilibrium for Reaction 7 shifts to the right. However, it is also known that current efficiency for aluminium deposition increases with increasing cathodic current density [10, 24] because sodium saturation of the graphite surface occurs more rapidly at higher currents, so that aluminium deposition can occur [23].

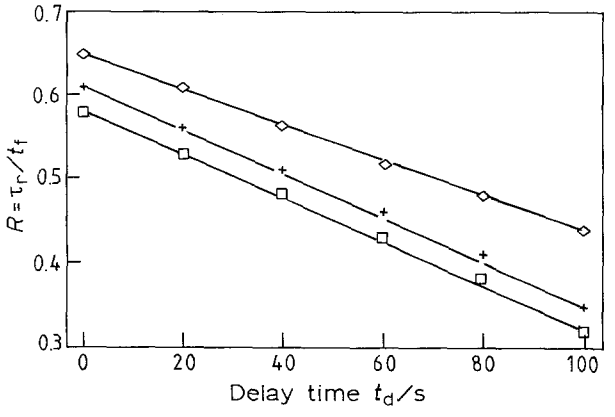

Fig. 8. Plots of (τ_r/t_f) against t_d for the COMP electrode in the unsaturated cryolite melt with 3 wt % Al_2O_3, 8 wt % AlF_3, and 5 wt % CaF_2 at 980° C. $A = 0.64\,cm^2$. Current, I: (□) 0.3, (+) 0.5, and (◇) 0.7 A.

Table 1. Dissolution rates of aluminium in alumina-saturated melts: CRC with delay results. Area of all electrodes = 0.64 cm², t_f = 100 s

Electrode	*Current density* i/A cm^{-2}	*Slope* $b/10^{-3}$ s^{-1}	r_d /10^{-7} mol cm^{-2} s^{-1}
COMP	0.47	2.89	4.68
COMP	0.78	2.58	6.98
COMP	1.09	2.53	9.56
COMP	1.56	2.29	12.49
ATJ graphite	0.47	3.00	4.86
ATJ graphite	0.78	3.20	8.78

3.3. *Current efficiency for aluminium deposition*

It is important to consider the effect of experimental variables on current efficiency to get a complete picture of the wettability of the composite cathodes by aluminium metal. From CRC studies [9, 23], it is not possible to determine the current efficiency of the cathodic process due to the interfering effect of metal dissolution during the forward and reverse pulse. The current efficiency for aluminium deposition can, however, be determined by combining the CRC and CRC with delay results. Considering the cathodic pulse, the total number of coulombs

$$Q_f = I_f t_f \quad (8)$$

and $Q_f = n_1F \times$ moles Al deposited $+ n_2F \times$ moles Na reduced. But the number of moles of Al deposited = the number of moles stripped during τ_r + the number of moles dissolved during $(t_f + \tau_r)$. That is

$$\text{Al deposited (moles)} = \frac{I_r\tau_r}{n_1F} + \frac{I_d(t_f + \tau_r)}{n_1F}$$

$$I_f t_f = \frac{I_r\tau_r + I_d(t_f + \tau_r)}{n_1F} + n_2F \times \text{moles Na reduced}$$

Current efficiency is defined as the ratio of the number of moles of aluminium deposited during t_f to the theoretical number of moles produced if there

Table 2. Aluminium dissolution rates in unsaturated melts: CRC with delay results. Area of all electrodes = 0.64 cm², t_f = 100 s

Electrode	*Current density* i/A cm^{-2}	*Slope* $b/10^{-3}$ s^{-1}	r_d /10^{-7} mol cm^{-2} s^{-1}
COMP	0.47	2.42	3.92
COMP	0.78	2.24	6.07
COMP	1.09	2.02	7.67
COMP	1.56	1.59	8.59
ATJ graphite	0.47	2.60	4.23
ATJ graphite	0.78	2.82	7.66
ATJ graphite	1.09	2.25	8.55

Table 3. Current efficiency for aluminium deposition in alumina-saturated melt. $A = 0.64\,cm^2$, $t_f = 100\,s$. Dissolution current obtained from CRC experiments

Current density $i/A\,cm^{-2}$	CE/%	
	COMP	Graphite
0.47	48	38
0.78	54	41
1.09	61	43
1.56	62	43

Table 5. Current efficiency for aluminium deposition in unsaturated melt. $A = 0.64\,cm^2$, $t_f = 100\,s$. Dissolution currents obtained from CRC experiments

Current density $i/A\,cm^{-2}$	CE/%	
	COMP	Graphite
0.47	66	43
0.78	69	46
1.09	73	47
1.32	75	48
1.56	77	50

were no competing reactions. That is

$$CE = \frac{\text{moles Al deposited during } t_f}{I_f t_f / n_1 F} \quad (9)$$

$$CE = \frac{\text{moles Al stripped during } \tau_r + \text{moles Al dissolved during } \tau_r}{I_f t_f / n_1 F}$$

In Equation 9 the number of moles of aluminium deposited durign t_f defines the number of moles of aluminium left at the electrode surface at the onset of the stripping (anodic) pulse, i.e. it takes into account the dissolution that occurs during the deposition process.

$$CE = \frac{I_r\tau_r + I_d\tau_r}{I_f t_f} = \frac{\tau_r(I_r + I_d)}{t_f I_f} = R\frac{(I + I_d)}{I}$$

The dissolution currents for above are obtained from r_d values obtained during CRC experiments and are based on a mass balance equation [9, 22, 23].

For CRC with delay:

$$CE = \frac{I_r\tau_r + I_d'(\tau_r + t_d)}{I_f t_f} \quad (10)$$

In this case I_d' is obtained from r_d values during CRC with delay experiments. Equations 9 and 10 enable the current efficiencies to be calculated, and the results are shown in Tables 3 to 6.

It is clear from Tables 3 to 6 that the current efficiency for aluminium deposition is higher in the unsaturated melt than in the Al_2O_3-saturated melt. These results are consistent with the results reported in Section 3.1. Further, the current efficiency values obtained for the COMP electrode under all conditions are much lower than the current efficiencies obtained in industrial cells [25]. This suggests that under these conditions aluminium is not able to form a thin, continuous film on the surface of the COMP cathodes. In an aluminium electrolysis study in a 100A laboratory cell with TiB_2/C-composite cathode [26] the current efficiency was found to be 88 to 92.7% for an unsaturated melt at a cathodic current density of $0.97\,A\,cm^{-2}$ and at an interpolar distance of 20 mm. It was also noticed that the molten aluminium had adhered firmly to the composite cathode, and this in turn reduced the rate of the back reaction and contributed towards the high current efficiencies. In our study current efficiency increases with current density in both the saturated and unsaturated melts. At low current density and long t_f ($t_f = 100\,s$) sufficient time is available for codepositing sodium to reach the surface of the electrode and to penetrate deep into the electrode substrate. A significant amount of sodium intercalation thus occurs as it takes time for aluminium activity to build-up to a fixed activity corresponding to the formation of a deposit and hence the current efficiency for aluminium deposition is low. However, at high cathodic current density sodium saturation occurs rapidly at the electrode surface so that aluminium deposition also occurs relatively

Table 4. Current efficiency for aluminium deposition in alumina-saturated melt. $A = 0.64\,cm^2$, $t_f = 100\,s$. Dissolution currents obtained from CRC with delay experiments

Current density $i/A\,cm^{-2}$	CE/%	
	COMP	Graphite
0.47	45	41
0.78	50	45
1.09	54	46
1.56	54	45

Table 6. Current efficiency for aluminium deposition in unsaturated melt. $A = 0.64\,cm^2$, $t_f = 100\,s$. Dissolution currents obtained from CRC with delay experiments

Current density $i/A\,cm^{-2}$	CE/%	
	COMP	Graphite
0.47	68	47
0.78	72	49
1.09	76	50
1.56	77	50

rapidly. Since the aluminium quickly wets the electrode surface, any codeposited sodium has to dissolve in aluminium first then diffuse through the aluminium layer to reach the composite substrate. Therefore, at high current densities the extent of sodium penetration into the substrate is relatively small, and hence the current efficiency for aluminium deposition is higher at higher current densities.

During their studies, Mazza *et al.* [6] studied the cathodic behaviour of two different composites, RHM 1 and RHM 2. The main constituents of RHM 1 were TiB_2–AlB_2–AlN and those for RHM 2 were TiB_2–AlN–BN. Photomicrographs showed that the extent of sodium penetration in RHM 1 was less than that in RHM 2. It was also noticed that RHM 1 was covered by a continuous film of liquid aluminium which limited sodium penetration while aluminium droplets were present in the RHM 2 material (due to the BN component being nonwettable by liquid aluminium), thereby allowing the deposition of sodium on large areas in direct contact with the bath. Furthermore, sodium penetration was shown to occur not in the interior of TiB_2 grains but at the grain boundaries.

The deposition behaviour on the COMP electrode seems to be similar to that observed by Mazza *et al.* at the RHM 2 electrode. For the COMP electrode, due to the nonwettability of the carbon matrix by molten aluminium, droplets of Al are formed on the TiB_2 particles instead of a thin, continuous film of molten aluminium. During electrolysis, accumulation of Na^+ near the electrode surface and the accessibility of carbon surface to sodium intercalation result in sodium codeposition. This in turn lowers the current efficiency for the aluminium deposition process. Overall, our results indicate that for the composite material investigated the wettable component (small TiB_2 particles) is unable to sustain an aluminium film over the nonwettable (coarse graphite filler) component. In another study with inert cathodes [26] it was found that aluminium globules formed at the surface of the vertical cathode during electrolysis, and some globules adhered to the surface of the cathode. Further studies of TiB_2/C composites with a wider range of compositions and granulometry are being undertaken to determine the optimum conditions for aluminium deposition [27].

4. Conclusions

The electrochemical techniques used in this study have provided a consistent set of results for TiB_2/C composite and ATJ graphite electrodes. The dissolution rate of electrolytically deposited aluminium at each electrode and under varying conditions is of the order of 10^{-7} mol cm^{-2} s^{-1}. In general, the dissolution rate increases with increasing current density.

It has also been seen that the dissolution rates are higher in alumina-saturated melts as compared to unsaturated melts. It was found that B_2O_3 and/or other oxides hinder the wetting process in alumina-saturated melts. The wetting process exhibited time dependency in alumina-saturated melts, and this was due to the removal of oxides and/or carbon from the electrode surface. It was found that wettability of the electrodes was enhanced by switching from an alumina-saturated melt to an unsaturated one.

For each electrode, sodium codeposition occurred with aluminium deposition, and this lowered the current efficiency for aluminium deposition. For graphite, sodium codeposition accounted for 50% of the applied current and for the COMP electrodes it accounted for about 30% at a current density of 0.8 A cm^{-2} in unsaturated melts. The current efficiencies for both electrodes were much lower in alumina-saturated melts than in unsaturated melts at all current densities, probably due to the poor wettability of aluminium on the electrode and because dissolution rates were higher in the former than in the latter. Overall, the current efficiencies were lower than those achieved in industrial cells where a continuous layer of molten aluminium covers the carbon cathode and reduces the rate of sodium deposition.

The two prewaves observed during cyclic voltammetry on the composite electrode are attributed to the reduction of titanium and boron on the electrode surface. Further, the results have indicated that the composite material employed here is not able to sustain a complete aluminium film over its surface and that a higher TiB_2 content or a change in granulometry would be required to improve the wettability of this material by molten aluminium.

Acknowledgements

Financial and technical support from Comalco Aluminium Ltd is gratefully acknowledged. The authors thank Comalco for permission to publish these results and appreciate the assistance of Paul Greenhill and Kevin Watson in providing samples and for useful discussions.

References

[1] K. Grjotheim and B. J. Welch, 'Aluminium Smelter Technology', Aluminium-Verlag, Dusseldorf (1980).
[2] K. Grjotheim and H. Kvande, 'Understanding the Hall–Heroult Process for Aluminium Production', Aluminium-Verlag, Dusseldorf (1986).
[3] D. Kasherman and M. Skyllas-Kazacos, *J. Appl. Electrochem.* **18** (1988) 863–8.
[4] J. C. Nixon, *Symposium Series Australas. Inst. of Min. Metall.* **43** (1985) 17–23.
[5] M. Reverdy, Third Australian Aluminium Smelting Technology Course, Sydney (1989).
[6] B. Mazza, A. Bonfiglioli, F. Gregu and G. Serravalle, *J. Electrochem. Soc.* **134**(5) (1987) 1187–91.
[7] L. G. Boxall and A. V. Cooke, 'Light Metals', AIME (1984).
[8] J. B. Todd, *J. Metals* **33** (1981) 42.
[9] E. Sum and M. Skyllas-Kazacos, *J. Appl. Electrochem.* **18** (1988) 731–8.
[10] K. Grjotheim, C. Krohn, M. Malinovsky, K. Matiasovsky and J. Thonstad, 'Aluminium Electrolysis', 2nd edn, Aluminium-Verlag, Dusseldorf (1982).
[11] E. Sum and M. Skyllas-Kazacos, Proceedings of the Seventh Electrochemistry Conference, Sydney (1988) pp. 87–190.
[12] Comalco Australia Limited, private communication.
[13] J. J. Duruz, G. Stehle and D. Landolt, *Electrochim. Acta* **26**(6) (1981) 771–9.

[14] D. W. McKee, *Carbon* **24**(6) (1986) 737.
[15] K. Grjotheim and K. Matiasovsky, *Aluminium* **59**(9) (1983) 687.
[16] Q. Zhuxian, Y. Yue, M. Zhang, K. Grotheim and H. Kvande, *Aluminium* **64**(12) (1988) 1254.
[17] S. C. Raj and M. Skyllas-Kazacos, *Electrochim. Acta* **37**(8) (1992) 1395.
[18] Q. Zhuxian, M. Zhang, Y. Yue, Z. Che, K. Grotheim and H. Kvande, *Aluminium* **64**(6) (1988) 606.
[19] D. Kubaschewski and C. B. Alcock, 'Metallurgical Thermochemistry', 5th edn, Pergamon, London (1979).
[20] A. J. Bard and L. R. Faulkner, 'Electrochemical Methods: Fundamental and Applications', Wiley, New York (1980).
[21] J. Thonstad and S. Rolseth, *Electrochim. Acta* **23** (1978) 223.
[22] E. Sum and M. Skyllas-Kazacos, *J. Appl. Electrochem.* **19** (1989) 485.
[23] E. Sum, Ph.D. Thesis, University of New South Wales (1988).
[24] J. J. Duruz and D. Landolt, *J. Appl. Electrochem.* **15** (1985) 393.
[25] A. Sterten, *ibid.* **18** (1988) 473.
[26] K. Grjotheim, *Metall. (Berlin)* **2**(6) (1988) 587.
[27] S. C. Raj and M. Skyllas-Kazacos, *J. Appl. Electrochem.*, submitted.